A Phase-Field Model Coupled with Large Elasto-Plastic Deformation: Application to Lithiated Silicon Electrodes

To cite this article: L. Chen *et al* 2014 *J. Electrochem. Soc.* **161** F3164

You may also like

- Large strain elasto-plasticity for diffuse interface models
  E Borukhovich, P S Engels, T Böhlke et al.

- Understanding the Mechanism of Stress Mitigation in Selenium-Doped Germanium Electrodes
  X. Wang, C. O. Yenusah, K. Tantratian et al.

- The phase field technique for modeling multiphase materials
  I Singer-Loginova and H M Singer

A Phase-Field Model Coupled with Large Elasto-Plastic Deformation: Application to Lithiated Silicon Electrodes

L. Chen,[a,*,z] F. Fan,[b] L. Hong,[a] J. Chen,[c] Y. Z. Ji,[a,**] S. L. Zhang,[d] T. Zhu,[b,*] and L. Q. Chen[a]

[a]*Department of Materials Science and Engineering, Pennsylvania State University, University Park, Pennsylvania 16802, USA*
[b]*Woodruff School of Mechanical Engineering, Georgia Institute of Technology, Atlanta, Georgia 30332, USA*
[c]*Department of Engineering, Pennsylvania State University, The Altoona College, Altoona, Pennsylvania 16601, USA*
[d]*Department of Engineering Science and Mechanics, Pennsylvania State University, University Park, Pennsylvania 16802, USA*

A phase-field model, accounting for large elasto-plastic deformation, is developed to study the evolution of phase, morphology and stress in crystalline silicon (Si) electrodes upon lithium (Li) insertion. The Li concentration profiles and deformation geometries are co-evolved by solving a set of coupled phase-field and mechanics equations using the finite element method. The present phase-field model is validated in comparison with a non-linear concentration-dependent diffusion model of lithiation in Si electrodes. It is shown that as the lithiation proceeds, the hoop stress changes from the initial compression to tension in the surface layer of the Si electrode, which may explain the surface cracking observed in experiments. The present phase-field model is generally applicable to high-capacity electrode systems undergoing both phase change and large elasto-plastic deformation.

As a promising anode material for lithium (Li)-ion batteries,[1–3] the theoretical Li capacity of Silicon (Si) is 4200 mAh/g (corresponding to the lithiated phase of $Li_{4.4}Si$), which is one order of magnitude larger than the commercialized graphite anode.[1,2] Recent experiments revealed that the lithiation of crystalline Si (*c*-Si) occurs through a two-phase mechanism, i.e., growth of lithiated amorphous Li_xSi (*a*-Li_xSi, $x \sim 3.75$) phase separated from the unlithiated *c*-Si phase by a sharp phase boundary of about 1 nm thick.[4–8] An abrupt change of Li concentration across the amorphous-crystalline interface (ACI) gives rise to drastic volume strain inhomogeneity. The resulting high stresses induce plastic flow, fracture, and pulverization of Si electrodes, thereby leading to the loss of electrical contact and limiting the cycle life of Li-ion batteries.[9–11]

Electrochemically driven mechanical degradation in high-capacity electrodes has stimulated enormous efforts on the development of chemo-mechanical models to understand how the stress arises and evolves in lithiated Si electrodes.[12–15] These chemo-mechanical models often treated the lithiation-induced stress as the diffusion-induced stress by considering Li diffusion in a solid-state electrode that results in the change of composition from its stoichiometric state. Deviation from stoichiometry usually results in a volume change that generates stress if the Li distribution is non-uniform. Early chemo-mechanical models only involved a unidirectional coupling. Namely, the diffusion-induced mechanical stress was considered, whereas the effect of mechanical stress on diffusion was ignored. Both experimental and computational studies, however, have shown that the mechanical stresses play an important role in the lithiation kinetics of Si electrodes.[4,6,16,17] Recently, fully coupled chemo-mechanical models were developed to incorporate the mechanical stress into the chemical potential.[18–22] In these models, the local stress modulates lithiation kinetics (reaction rate and diffusivity),[4,6,23] and in turn, lithiation kinetics regulates the stress generation in lithiated Si electrodes.[6] However, most efforts of coupling the diffusion with stress were made in the elastic regime of Si electrodes.

Motivated by recent experimental observations of drastic morphological changes in lithiated Si electrodes, more sophisticated models have recently been developed to account for the large elasto-plastic deformation coupled with Li diffusion.[12,15,18,19,21,24] Based on non-equilibrium thermodynamics, Zhao et al.[15,21] considered the coupled large plastic deformation and lithiation in a spherical Si electrode. Bower et al.[12,18] developed a theoretical framework to incorporate finite deformation, diffusion, plastic flow, and electrochemical reaction in lithiation of Si electrodes. Such models treated Li diffusion in a single phase with a gradual variation of Li concentration, which is inconsistent with the two-phase lithiation mechanism uncovered by the recent in situ transmission electron microscopy (TEM) experiments. Huang et al.[25,26] and Yang et al.[27,28] developed a non-linear concentration-dependent diffusion model in which Li diffusivity was treated as a non-linear function of Li concentration so as to effectively generate a sharp phase boundary. However, such non-linear diffusion model, implemented in a general finite element framework, failed to provide a characteristic length scale as the interface thickness varied with the lithiation time. Cui et al.[24] and Liu et al.[4] studied the lithiation of Si by considering the interfacial chemical reactions and bulk diffusion as two sequential processes. But they did not directly simulate the concurrent processes of Li diffusion and reaction.

Phase-field method (PFM) has been applied to a vast range of phenomena in materials processes, e.g., solidification,[29] solid-state phase transformation,[30] recrystallization,[31] and grain growth.[32,33] PFM is formulated based on the theory of irreversible thermodynamics, and is advantageous in addressing the time-dependent evolving morphologies and describing the complex microstructure evolution process. In particular, the diffuse interface between adjacent phases can be conveniently captured by a gradient term without the need of cumbersome tracking of a sharp interface in every step of numerical simulations. The early attempt along this line was to couple PFM with a linear elasticity model by Van de Ven et al.,[34] who investigated the effect of coherency strains on phase stability in $LiFePO_4$. Later, Bazant et al.[35,36] developed a thermodynamically consistent PFM, coupled with the linear elasticity, to simulate the non-linear Butler-Volmer reaction kinetics. More recently, Anand et al.[37] proposed a general formalism to couple phase-field with large elasto-plastic deformation.

Di Leo et al.[38] subsequently implemented this formalism with a numerical approach to simulate the LiFePO$_4$ electrode material. However, these phase-field models either assume linear elastic deformation that is not applicable to the Si electrodes undergoing large plastic deformation during lithiation, or are still at the early stage of development without numerical implementations for the high-capacity electrode materials.

In this paper, we aim to develop a phase-field model coupled with large elasto-plastic deformation. We employ this model to simulate lithiation of Si electrodes, which involve both the large geometrical change and phase change. The Li-poor/Li-rich phase boundary is naturally captured without any special treatment (e.g., usage of an interfacial domain). We solve the elasto-plastic equilibrium equations in every step of temporal phase-field evolution by the finite element method (FEM). Our phase-field model is numerically implemented in the physical space such that it is well suited to study the effects of complex geometries and boundary conditions. Moreover, this model is thermodynamically consistent and enables the full chemo-mechanical coupling.

Problem Description

We study a simple model problem: lithiation of a nanowire electrode with a cross section of radius A, as shown in Figure 1a. Upon lithiation, the Li distribution becomes non-uniform in the radial direction, but retains circular symmetry. The insertion of Li atoms causes the nanowire electrode to swell to a radius a, as shown in Figure 1b. The non-uniform distribution of Li generates the stress inside the nanowire. A key feature of lithiation in the c-Si electrode is the formation of a phase boundary of 1 nm in thickness,[4–8,11] which separates the Li-rich and Li-poor phases (see Figure 1c). The electron diffraction pattern indicates that the Li-rich phase is a-Li$_{3.75}$Si. This composition is further confirmed by the apparent volume expansion close to that of c-Li$_{3.75}$Si as well as the dynamic formation of Li$_{3.75}$Si nanocrystals within the amorphous phase.[4,6,9] In the c-Si core the lattice expansion remains negligibly small, indicating the low Li concentration and accordingly the Li-poor phase therein. Across the sharp phase boundary, Li concentration changes abruptly. In other words, the Li-poor phase does not continuously transform to the Li-rich one with a gradual change of Li content, and lithiation is mediated by the phase boundary migration. The sharp phase boundary plays a critical role in stress generation and fracture in c-Si during lithiation.[4,6] Hence, it is important to develop a fully coupled chemo-mechanical model to simulate the co-evolution of phase, morphology and stress during the lithiation process.
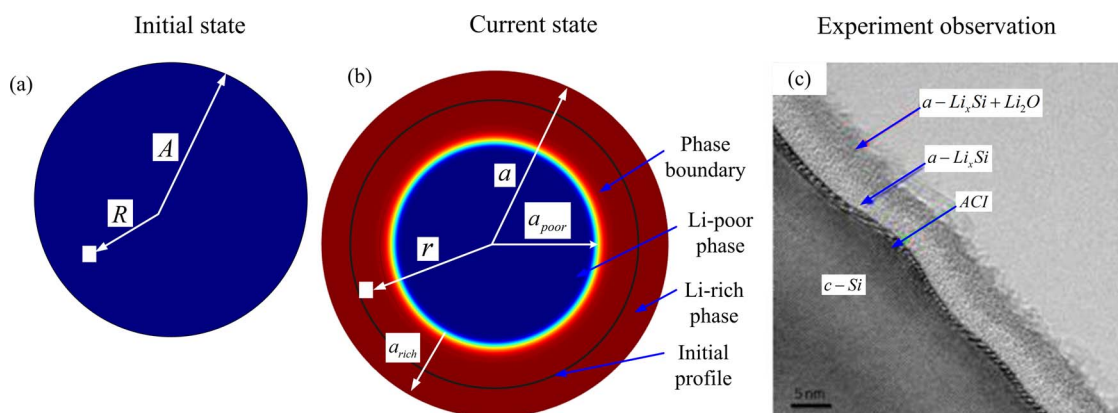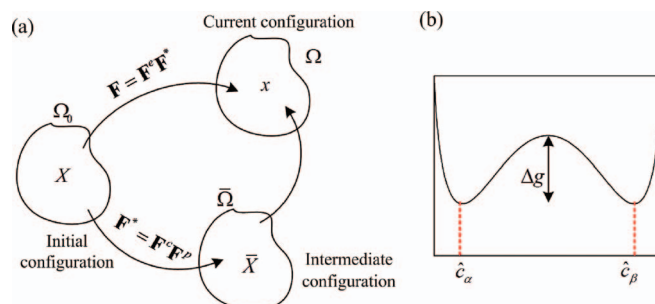
Figure 2. Schematic diagram showing (a) decomposition of deformation gradient and definition of intermediate configuration; (b) double well chemical free energy function.

A Constitutive Model of Lithiation-Induced Elasto-Plastic Deformation

In this section, a constitutive model is developed to characterize the large elasto-plastic deformation in a lithiated Si electrode.

Kinematics of deformation.— The kinematics for any material point in a continuum can be described by a continuous displacement field **u** given by

$$\mathbf{u} = \mathbf{x} - \mathbf{X}, \quad [1]$$

where **x** is the position of the material point at time t and **X** is the initial position at $t = 0$. The deformation gradient is defined as $\mathbf{F}(\mathbf{X}, t) = \nabla_{\mathbf{X}}\mathbf{x}$, where $\nabla_{\mathbf{X}}$ is the gradient operator with respect to **X**.

In continuum mechanics, a multiplicative decomposition of the deformation gradient is typically assumed

$$\mathbf{F} = \mathbf{F}^e \mathbf{F}^*, \quad \mathbf{F}^* = \mathbf{F}^c \mathbf{F}^p, \quad [2]$$

where $\mathbf{F}^c$ represents the chemically-induced deformation gradient due to the compositional inhomogeneity, $\mathbf{F}^p$ is the plastic deformation gradient, and $\mathbf{F}^e$ is the elastic deformation gradient. Eq. 2 indicates that the total deformation can be considered as an accumulation of an inelastic deformation followed by an elastic deformation. The state of the material point after inelastic deformation is named as the intermediate state, as shown in Figure 2a. In particular, such state is stress free and is not necessarily compatible in kinematical sense.[39]

Following Eq. 2, the total Lagrange strain can be given as

$$\mathbf{E} = \frac{1}{2}(\mathbf{F}^{\mathrm{T}}\mathbf{F} - \mathbf{I}) = (\mathbf{F}^c\mathbf{F}^p)^{\mathrm{T}}\mathbf{E}^e\mathbf{F}^c\mathbf{F}^p + (\mathbf{F}^p)^{\mathrm{T}}\mathbf{E}^c\mathbf{F}^p + \mathbf{E}^p, \quad [3]$$

Figure 1. Schematic diagram showing a typical lithiation process from (a) the initial state with a lithiation-free and stress-free silicon nanowire electrode to (b) the current state in which the electrode is partially lithiated with the sharp phase boundary and a stress field is developed. The model is consistent with (c) In situ TEM observed core-shell structure in a partially lithiated Si electrode, where the crystalline core (c-Si) is surrounded by the amorphous shell (a-Li$_x$Si). The amorphous-crystalline interface (ACI), i.e., the phase boundary separating the amorphous lithiated shell and the unlithiated crystalline core, is atomically sharp ($\sim$1 nm).[4–8]

where

$$\mathbf{E}^e = \frac{1}{2}[(\mathbf{F}^e)^{\mathrm{T}}\mathbf{F}^e - \mathbf{I}] \quad \mathbf{E}^c = \frac{1}{2}[(\mathbf{F}^c)^{\mathrm{T}}\mathbf{F}^c - \mathbf{I}]$$

$$\mathbf{E}^p = \frac{1}{2}[(\mathbf{F}^p)^{\mathrm{T}}\mathbf{F}^p - \mathbf{I}] \qquad [4]$$

are, respectively, the elastic, chemical, and plastic strain tensors.

Stress equilibrium.— As the long-range Li diffusion is typically much slower than the local stress relaxation, a mechanical equilibrium holds at any time, i.e.

$$\sigma^0{}_{ij,j}(\mathbf{X}) = 0, \qquad [5]$$

where $\boldsymbol{\sigma}^0(\mathbf{X})$ is the first Piola-Kirchhoff (P-K) stress tensor,

$$\boldsymbol{\sigma}^0 = \frac{\partial W(\mathbf{F}, \hat{c})}{\partial \mathbf{F}} = \frac{\partial W(\mathbf{F}, \hat{c})}{\partial \mathbf{E}^e}\frac{\partial \mathbf{E}^e}{\partial \mathbf{F}^e}\frac{\partial \mathbf{F}^e}{\partial \mathbf{F}} = \frac{\partial W(\mathbf{F}, \hat{c})}{\partial \mathbf{E}^e}\mathbf{F}^e(\mathbf{F}^p)^{-1}(\mathbf{F}^c)^{-1}.$$
$$[6]$$

We denote c and $c_{\max}$ as the current and maximum true Li concentration in the lithiated Si, respectively. The normalized Li concentration is defined as $\hat{c} = c/c_{\max}$. Note that $\hat{c}$ represents the fraction of lithiation at a material point relative to its fully lithiated state, which is independent of the deformation gradient $\mathbf{F}$ of the associated material point. For brevity, $\hat{c}$ will still be called the Li concentration in the rest of this paper.

Elasto-plastic deformation.— We take the total deformation gradient $\mathbf{F}$ and the concentration $\hat{c}$ as the independent variables, thus, the elastic energy density in the Lagrangian description (initial configuration) $W_{el}(\mathbf{F}, \hat{c})$ can be written as

$$W_{el}(\mathbf{F}, \hat{c}) = \frac{J^c E}{2(1 + v)}(tr(\mathbf{E}^e\mathbf{E}^e) + \frac{v}{1 - 2v}[tr(\mathbf{E}^e)]^2), \qquad [7]$$

where E and v are, respectively, Young's modulus and Poisson's ratio for the Li$_x$Si phase, both of which depend on $\hat{c}$, and J^c is the chemical deformation Jacobian. The elastic energy density corresponding to the intermediate state $w_{el}(\mathbf{F}, \hat{c})$ is

$$w_{el}(\mathbf{F}, \hat{c}) = (J^*)^{-1}W_{el}(\mathbf{F}, \hat{c}), \qquad [8]$$

where J^* is the Jacobian that transforms an infinitesimal element of volume in the initial configuration to the corresponding fraction of volume in the intermediate configuration, i.e.

$$J^* = \det(\mathbf{F}^*). \qquad [9]$$

Assuming the plastic deformation is volume preserving, i.e., the plastic deformation Jacobian $J^p = \det(\mathbf{F}^p) = 1$, one can write

$$w_{el}(\mathbf{F}, \hat{c}) = (J^*)^{-1}W_{el}(\mathbf{F}, \hat{c}) = (J^c)^{-1}W_{el}(\mathbf{F}, \hat{c}). \qquad [10]$$

We assume the chemical deformation is isotropic that is given by

$$\mathbf{F}^c = \beta\hat{c}\mathbf{I}, \qquad [11]$$

where β is the coefficient of chemical expansion associated with Li insertion, and $\mathbf{I}$ is the second-order identity tensor.

Next, we turn to the constitutive law (i.e., the flow rule) of plastic deformation. The rate of plastic stretch is expressed as

$$\mathbf{D}^p = 1/2(\mathbf{L}^p + \mathbf{L}^{pT}), \qquad [12]$$

where $\mathbf{L}^p$ corresponds to the plastic part of the spatial gradient of velocity, given as

$$\mathbf{L}^p = \mathbf{F}^e\mathbf{F}^c\dot{\mathbf{F}}^p(\mathbf{F}^p)^{-1}(\mathbf{F}^c)^{-1}(\mathbf{F}^e)^{-1}. \qquad [13]$$

The plastic stretch rate, $\mathbf{D}^p$, obeys the associated J_2-flow rule. Namely, plastic yielding occurs when the equivalent stress, $\tau_e = \sqrt{\frac{3}{2}\boldsymbol{\tau}' : \boldsymbol{\tau}'}$, reaches the yield strength, $\boldsymbol{\sigma}_y$. Here $\boldsymbol{\tau}'$ is the deviatoric part of the Kirchhoff stress tensor $\boldsymbol{\tau}$, i.e., $\boldsymbol{\tau}' = \boldsymbol{\tau} - tr(\boldsymbol{\tau})\mathbf{I}/3$. Note that the Kirchhoff stress tensor is related to the first P-K stress tensor as $\boldsymbol{\tau} = \mathbf{F}\boldsymbol{\sigma}^0(\mathbf{X})$. Also, the Cauchy stress is expressed as $\boldsymbol{\sigma} = J^{-1}\mathbf{F}\boldsymbol{\sigma}^0(\mathbf{X})$, where J corresponds to the total deformation Jacobian.

In the J_2-flow theory, the plastic stretch rate is given by

$$\mathbf{D}^p = \frac{3}{2}\frac{\boldsymbol{\tau}'}{\tau_e}D_{eq}^p, \qquad [14]$$

where $D_{eq}^p = \sqrt{2\mathbf{D}^p : \mathbf{D}^p/3}$ is the equivalent plastic stretch rate.

The lithiated Si electrode is modeled as an isotropic elasto-plastic material with a simple linear hardening rule

$$\sigma_y = \sigma_{y0} + H\bar{\varepsilon}^p, \qquad [15]$$

where σ_{y0} denotes the initial yield strength, H is the hardening modulus of the material, and $\bar{\varepsilon}^p$ is the total accumulated equivalent plastic stretch, given by

$$\bar{\varepsilon}^p = \int_t D_{eq}^p dt. \qquad [16]$$

In the above expressions, all the field variables such as the Green-Lagrange elastic strain tensor $\mathbf{E}^e$, the first P-K stress $\boldsymbol{\sigma}^0$, and the plastic stretch rate $\mathbf{D}^p$ are functions of the deformation gradient tensor $\mathbf{F}$. Once $\mathbf{F}$ is known, $\mathbf{E}^e$ can be calculated from Eq. 4, $\boldsymbol{\sigma}^0$ from Eqs. 6 and 7, and $\mathbf{L}^p$ from Eq. 13.

Phase-Field Model

A phase-field model usually relies on the continuous order parameter such as local concentration. In a lithiated Si electrode, Li atoms are assumed to reside in the lattice sites of a crystalline phase of Li$_x$Si - the actual phase could be amorphous, but with the same composition. The concentration field, as a conserved property, evolves by long-range diffusion. Hence, in principle, a description of diffusion and phase boundary migration within the electrode material requires two fields: the Li concentration field describing the local degree of lithiation, and a phase-field that distinguishes the crystalline state and the amorphous state. For simplicity, in this paper both the local degree of lithiation and the structural difference between the crystalline and amorphous states together are described by a single Li concentration field. The temporal and spatial evolution of the Li concentration field is obtained by solving the Cahn-Hilliard equation. It should be emphasized that since every material point in lithiated Si can locally undergo very large volume expansion up to about 300%, care must be taken in choosing the appropriate field variable that accounts for lithiation-induced large strains. In this work, we choose the normalized Li concentration $\hat{c}$ as the field variable, so as to facilitate the coupling between the phase-field and constitutive models.

In a phase-field model, the free energy functional G is the total free energy of an inhomogeneous system,

$$G = \int_V \left[f_{ch}(\hat{c}) + \frac{\kappa}{2}(\nabla\hat{c})^2 + f_{el}(\mathbf{F}, \hat{c}) + f_{pl}(\mathbf{F}) \right] dV, \qquad [17]$$

where $f_{ch}(\hat{c})$, $f_{el}(\mathbf{F}, \hat{c})$ and $f_{pl}(\mathbf{F})$ represent the local energy density from the chemical, elastic and plastic contribution, respectively. The Li concentration gradient term $\kappa/2(\nabla\hat{c})^2$ contributes to the phase boundary energy. More specifically, $f_{ch}(\hat{c})$ is the chemical free energy density of the stress-free state and is given by a double-well function

$$f_{ch}(c) = c_{\max}RT\left[\hat{c}\ln(\hat{c}) + (1 - \hat{c})\ln(1 - \hat{c}) + \Omega\hat{c}(1 - \hat{c})\right]. \qquad [18]$$

While Eq. 18 is a regular solution model, the lithiated Si is amorphous and cannot be simply characterized as a regular solution. Hence we only take Eq. 18 as a mathematic function with double energy wells, which represent the Li-poor and Li-rich phases, respectively. The dimensionless parameter Ω controls the profile of the double-well energy function. In addition, $f_{el}(\mathbf{F}, \hat{c})$ and $f_{pl}(\mathbf{F})$ are, respectively, the elastic and plastic energy densities arising from the inhomogeneous lithiation

$$f_{el}(\mathbf{F}, \hat{c}) = W_{el}(\mathbf{F}, \hat{c}) \qquad [19]$$

and

$$f_{pl}(\mathbf{F}) = \int \Delta W_{pl}(\mathbf{F})dt, \qquad [20]$$

where ΔW_{pl} corresponds to the increment of the plastic energy density, given by

$$\Delta W_{pl}(\mathbf{F}) = \boldsymbol{\tau} : \mathbf{D}^p. \qquad [21]$$

The Li potential μ is defined as the variational derivative of G,

$$\mu = \frac{\delta G}{\delta \hat{c}} = \frac{\partial f_{ch} + \kappa/2(\nabla \hat{c})^2}{\partial \hat{c}} + \frac{\partial f_{el}}{\partial \hat{c}} + \frac{\partial f_{pl}}{\partial \hat{c}} = \mu_{ch} + \mu_{el} + \mu_{pl}, \qquad [22]$$

where the chemical driving force, including the gradient term, is given by

$$\mu_{ch} = \frac{\partial f_{ch}}{\partial \hat{c}} - \kappa \nabla^2 \hat{c} = c_{\max} RT \left[\Omega(1 - 2\hat{c}) + \ln \frac{\hat{c}}{1 - \hat{c}} \right] - \kappa \nabla^2 \hat{c}. \qquad [23]$$

The elastic driven force μ_{el} is given by

$$\mu_{el} = \frac{\partial f_{el}(\mathbf{F}, \hat{c})}{\partial \hat{c}} = \frac{\partial J^c w_{el}(\mathbf{F}, \hat{c})}{\partial \hat{c}} = \frac{\beta}{J^c} \Sigma_{kk} + J^c \frac{\partial w_{el}(\mathbf{F}, \hat{c})}{\delta \hat{c}}, \qquad [24]$$

where Σ_{kk} is the conventional Eshelby's stress tensor,[40,41] as

$$\Sigma_{kk} = 3 J^c w_{el}(\mathbf{F}, \hat{c}) - \tau_{kk}. \qquad [25]$$

Regarding Eq. 24, the terms of the order $\boldsymbol{\sigma}^0 \mathbf{E}$ or higher can be neglected if both the elastic and chemical strains are small, such that $J^c = 1$ and different stress measures are equivalent. Under these conditions, one can show that Eq. 24 can be reduced to the classic equation by Larche and Cahn[42]

$$\mu_{el} = -\beta \sigma_{kk} + \frac{\partial C_{ijkl}}{\delta \hat{c}} E_{ij} E_{kl}. \qquad [26]$$

We assume that the plastic energy density is independent of $\hat{c}$, so that

$$\mu_{pl} = \frac{\partial f_{pl}(\mathbf{F})}{\partial \hat{c}} = 0. \qquad [27]$$

The Li diffusion equation is derived by

$$\frac{\partial \hat{c}}{\partial t} = -\nabla J_{flux}, \qquad [28]$$

with the concentration flux J_{flux} related to the Li potential μ according to

$$J_{flux} = -M_{\text{Li}}(\hat{c}) \nabla \mu, \qquad [29]$$

where M_{Li} is the Li mobility tensor that is in general a function of Li concentration $\hat{c}$, as

$$M_{\text{Li}}(\hat{c}) = \frac{D}{\partial f_{ch}^2(\hat{c}) / \partial \hat{c}^2} = \left(\frac{D}{c_{\max} RT} \right) [\hat{c}(1 - \hat{c})], \qquad [30]$$

where D is the inter-diffusion coefficient.

Combining Eqs. 22–30 yields the Cahn-Hilliard type of phase-field equation

$$\frac{\partial \hat{c}}{\partial t} = \nabla \cdot M_{\text{Li}}(\hat{c}) \nabla \left\{ c_{\max} RT \left[\Omega(1 - 2\hat{c}) + \ln \frac{\hat{c}}{1 - \hat{c}} \right] - \kappa \nabla^2 \hat{c} + \mu_{el} \right\}. \qquad [31]$$

Numerical Implementation

The phase-field equations coupled with the constitutive equations of elasto-plastic deformation are solved by using a FEM-based numerical method through a commercial software package, COMSOL. Compared to the commonly used spectral method for the phase-field simulations, the FEM-based approach facilitates the integration of the combined phase-field and mechanics equations, such that it is well suited to solve problems with large elasto-plastic deformation and finite-sized geometry of an arbitrary shape under various initial and boundary conditions.

Decomposition of the Cahn-Hilliard formulation.— The Cahn-Hilliard formulation involves a fourth-order, non-linear parabolic equation. Unfortunately, the present FEM-based numerical platform is not directly applicable to the fourth-order equations. Hence, we deal with the Cahn-Hilliard equation by decomposing it into a set of two second-order equations: one is the parabolic equation expressed as

$$\frac{\partial \hat{c}}{\partial t} = \nabla \cdot M_{\text{Li}}(\hat{c}) \nabla \mu, \qquad [32]$$

and the other is

$$\mu = c_{\max} RT \left[\Omega(1 - 2\hat{c}) + \ln \frac{\hat{c}}{1 - \hat{c}} \right] - \kappa \nabla^2 \hat{c} + \mu_{el}. \qquad [33]$$

The occurrence of two phases results from a non-convex, double-well chemical free energy of Eq. 18 shown in Figure 2b. Experiments show that the Li-rich phase likely consists of amorphous $Li_{3.75}Si$ at room temperature, whereas the theoretical lithiation product is $Li_{4.4}Si$. Hence, the normalized Li concentration for the actual Li-rich phase is $3.75/4.4 = 0.872$. Thus, the coefficient Ω in Eq. 18 is chosen as $\Omega = 2.6$ in order to enforce the Li-rich phase to take such a concentration value, as shown in Figure 2b.

Boundary conditions.— In the present numerical platform, two types of boundary conditions are imposed, one corresponds to the Cahn-Hilliard (phase-field) equation, and the other to the mechanical stress equilibrium. For the former, since the governing equation is of the fourth-order, two boundary conditions are required to solve the resulting two second-order partial differential equations after decomposition.

$$\begin{cases} \hat{c} = \hat{c}_\beta \\ -\mathbf{n} \cdot \mu = 0 \end{cases} \quad \text{on } \Gamma^d, \qquad [34]$$

where $\mathbf{n}$ is the outward normal at the outer surface Γ^d of the Si electrode.

1) In experiments, Li was observed to quickly cover the outer surface of the Si nanowire electrode due to its much lower migration barriers on the Si surface than in the bulk.[9,10,43] We thus prescribe a Dirichlet boundary condition that assumes a saturated Li concentration of $\hat{c}_\beta$, corresponding to Li-rich phase (see Figure 2b), on the Si outer surface throughout the lithiation process;
2) The flux of potential is set to be zero on the Si electrode outer surface Γ^d.

Further, regarding the mechanics boundary conditions, we assume the outer surface Γ^d of the Si electrode is traction free

$$-\mathbf{n} \cdot \boldsymbol{\sigma} = 0 \quad \text{on } \Gamma^d. \qquad [35]$$

Due to circular symmetry, only a quarter of each Si nanowire electrode is simulated and the symmetrical boundary conditions are imposed in order to reduce the computational cost.

Transformation to the weak form.— Plane 3-node triangular elements with four degrees of freedom (c, μ, u_i) per node are used in the 2D discretization. Time integration is accomplished using an implicit first-order scheme. The weak (variational) form of the problem reads:

find $\mathbf{d} = [\hat{c}, \mu, u_i]^T \in \mathcal{V} \times \mathcal{V}$ where

$$\mathcal{V} = \{ \mathbf{d}(\mathbf{X}, t) | \mathbf{d}(\mathbf{X}, t) \in \mathbf{H}^2, \ \mathbf{d}(\mathbf{X}, t) = \mathbf{d}(\mathbf{X}, t) \text{ on } {}^0\Gamma^d \}, \qquad [36]$$

such that:

$$\int_{{}^0\Omega} \dot{\hat{c}} \cdot q \ d^0\Omega + \int_{{}^0\Omega} M_{Li} \nabla \mu \cdot \nabla q \ d^0\Omega = 0 \qquad \forall q \in \mathcal{V} = \qquad [37]$$

Table I. Phase-field simulation parameters and their normalized values.

Parameter	Real value		Normalized value	
	Symbol	Value	Symbol	Value
Mobility	M	$2.186 \times 10^{-26} \mathrm{m^5/J \times s}$	$M^* = M/M^N$	10.0
Gradient energy coefficient	κ	$2.0 \times 10^{-9} \mathrm{J/m}$	$\kappa^* = \kappa/(RT c_{max} \times l^2)$	0.0005
Expansion coefficient	β	0.5874		0.5874
Elastic modulus	E	$160 \sim 40$ GPa	$\sigma_y^* = \sigma_y/RT c_{max}$	175
Poisson's ratio	v	$0.24 \sim 0.22$		0.24
Yield strength	σ_y	1.5 GPa	$\sigma_y^* = \sigma_y/RT c_{max}$	1.64
Strain hardness	H	1.0 GPa	$H^* = H/RT c_{max}$	1.092
Radius	A	70 nm	$A^* = A/l$	1
Time step	Δt	2.45 s	$\Delta t^* = \Delta t/(l^2/M^N RT c_{max})$	10^{-3}

$$\int_{0\Omega} \mu \cdot p \, d^0\Omega + \int_{0\Omega} \kappa \nabla \hat{c} \cdot \nabla p \, d^0\Omega \qquad \forall p \in \mathcal{V} =$$

$$-\int_{0\Omega} \left[c_{max} RT \left(\Omega(1 - 2\hat{c}) + \ln \frac{\hat{c}}{1 - \hat{c}} \right) + \mu_{el} \right] \cdot p \, d^0\Omega = 0$$

$$[38]$$

$$\int_{0\Omega} \dot{\sigma}_{ij}^0 \cdot \nabla \left(\frac{\partial v_j}{\partial X_i} \right) d^0\Omega = 0 \qquad \forall v_i \in \mathcal{V} =$$

$$[39]$$

where the superscript 0 indicates that the integration extents are in the reference (initial) configuration. Rates are indicated by the superposed dot. The prefix ∇ on q, p, v_i identifies the test (arbitrary virtual) function.

Numerical Results

Model parameters.— We adopt an isotropic elasto-plastic model along with a linear hardening law to describe the lithiation-induced deformation in Si electrodes, as described before. For material properties in the elastic range, Young's modulus and Poisson's ratio are both assumed to vary linearly with Li concentration from 160 to 40 GPa and from 0.24 to 0.22,[20,43] respectively. However, the material properties in the plastic range are not available. Hence, we use typical values for the yield strength $\sigma_y = 1.5$ GPa, and the hardening modulus $H = 1.0$ GPa, which provide a reasonable fit to recent experiments.[1,17,44]

The coefficient of compositional expansion is taken as $\beta = 0.5874$ which yields a volume increase of 300% in the fully lithiated phase. The gradient energy coefficient κ is assumed to be 2.0×10^{-9} Jm^{-1}. The mobility $M^0 = D/c_{max}RT$ for the Cahn-Hilliard equation (see Eq. 30) is chosen to be 2.186×10^{-26} m^5/J · s, which corresponds to the inter-diffusion coefficient D of 2×10^{-17} m^2/s. The initial radius of Si electrode is $A = 70$ nm. The time step Δt for integration is taken as 2.45 s.

In both phase-field and non-linear diffusion models, the equations are solved in their dimensionless forms. Both moduli and stresses are normalized by $c_{max}RT$ that is estimated as follows. The volume of one mole Si atoms in solid is given by $V = m_{si}/\rho_{si} = 1.2 \times 10^{-5}$ m^3/mole, where m_{si} and ρ_{si} are molar mass and density of Si, respectively. It is known that the compound with maximum Li concentration among all the possible Li/Si compounds during the electrochemical reactions is Li$_{4.4}$Si. Thus, the maximum nominal Li concentration c_{max} is determined by $c_{max} = 4.4/V = 0.3667 \times 10^6$ mole/m^3, thus $c_{max}RT = 0.915$ GPa.

The length parameters are normalized by $l = 70$ nm, yielding a normalized Si electrode radius of $A^* = A/l = 1$. The mobility M^0 is normalized by a factor $M^N = 2.186 \times 10^{-27}$ m^5/J · s as $M^* = M^0/M^N = 10.0$. To further normalize time, the factor $t_d = l^2/M^N c_{max}RT$ is employed as $\Delta t^* = \Delta t/t_d = 10^{-3}$. The physical parameters and their normalized value are summarized in Table I.

Validation of the phase-field model.— In this work, we focus on validating the phase-field model so as to provide a solid basis for its applications to the complex boundary-value problems in the future. Figure 3 shows the radial distribution of normalized Li concentration, $\hat{c}$, at different lithiation times of $t = 500, 5000, 9000\Delta t$. A sharp interface is simulated between the Li-poor and Li-rich phases at each snapshot, thus yielding a core/shell structure as experimentally observed during lithiation of Si nanowires.[3,5] Further, the lithiation front distance at the time interval of $t = 5000 - 9000\Delta t$ is markedly smaller than that from $t = 500 - 5000\Delta t$, indicating the slowing down of lithiation as lithiation proceeds, which agrees with the experimentally observed self-limiting lithiation phenomenon.[4,6] The lithiation-induced compressive stress at the reaction front is expected to play a role in lowering the lithiation rate.[4,6] A systematic investigation of such retardation effect will be reported in a forthcoming publication.

We next compare the radial stress distributions predicted from the present phase-field with the previously developed non-linear diffusion model.[25] As shown in Figure 4, three stress components are included, i.e., the radial stress, σ_r, the hoop stress σ_θ, and the von Mises effective stress, $\sigma_e = |\sigma_r - \sigma_\theta|$. Specifically, Figure 4a and 4b show the results of the present phase-field model at $t = 500\Delta t$ and $t = 9000\Delta t$, respectively, giving the phase boundary position at $R/A = 0.85$ and $R/A = 0.5$. Figure 4c and 4d show the corresponding numerical results from the non-linear diffusion model.[25]

Figure 4a and 4c are representative of the early stage of lithiation, while Figure 4b and 4d the late stage of lithiation. The present phase-field model exhibits the overall consistency with the previous non-linear diffusion model. The small difference arises possibly from the fact that a rate-dependent plasticity model without strain hardening was employed in the previous non-linear diffusion model, whereas a rate-independent plasticity model with linear (but weak) strain hard-
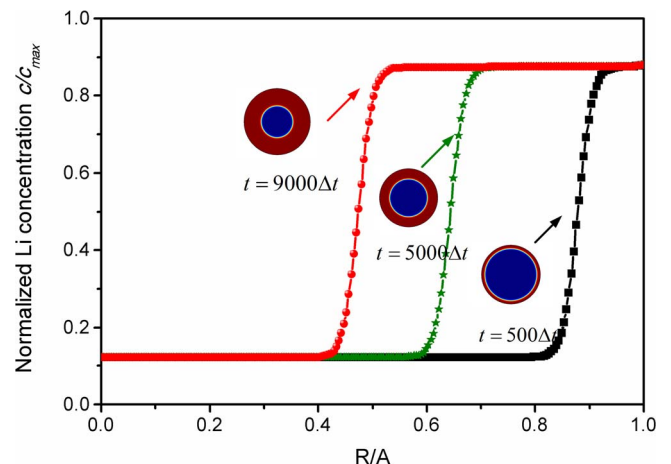

Figure 3. Radial distribution of Li concentration, $\hat{c} = c/c_{max}$, at different lithiation times.
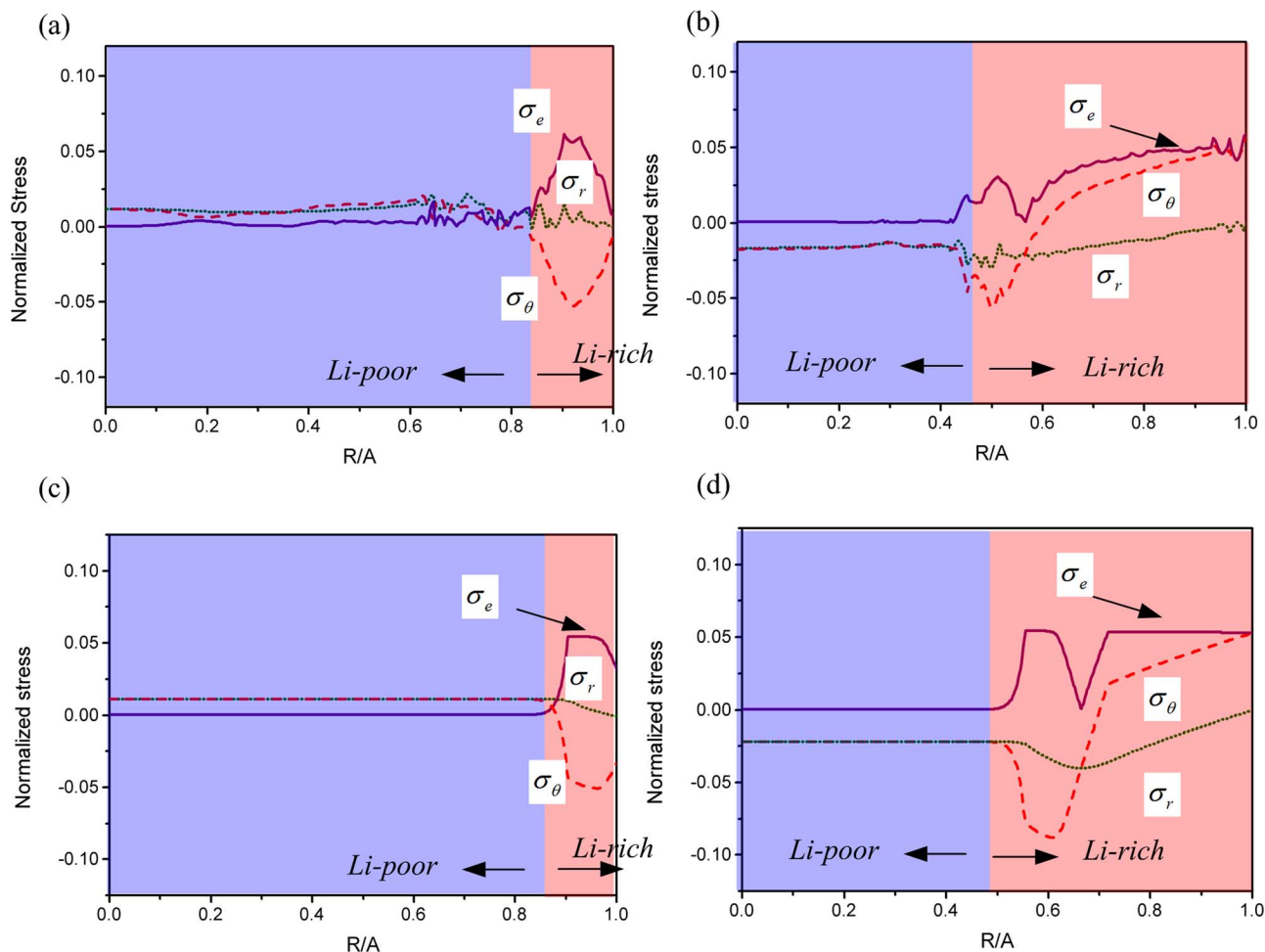
Figure 4. Comparison of radial distributions of the von Mises effective stress, σ_e, radial stress, σ_r and hoop stress σ_θ obtained by: (a) the phase-field model at time of $t = 500\Delta t$ with phase boundary located approximately at $R/A = 0.85$, (b) the phase-field model at time of $t = 9000\Delta t$ with phase boundary around at $R/A = 0.5$, (c) the non-linear diffusion model[25] with phase boundary at $R/A = 0.85$ and (d) the non-linear diffusion model[25] with phase boundary at $R/A = 0.5$. All the stress components are normalized by Young's modulus of Si, E_{si}.

ening is used in the present phase-field model, that is necessary for numerical stability. Furthermore, the mesh density and geometry could contribute to numerical differences between the two models, e.g., the phase-field results exhibit small fluctuations in stress distribution and a further improvement on numerical stability is necessary in the future.

For completeness, the main findings from Figure 4 are summarized as follows:

1)　As lithiation proceeds to the late stage, Figure 4b and 4d show that the hoop stress σ_θ is tensile in the surface layer of a Si electrode, opposite to the compressive hoop stress at the early stage, as shown in Figure 4a and 4c. This reversal of hoop compression to tension explains the surface cracking of Si electrodes as observed in in situ lithiation experiments.

2)　The traction-free boundary condition dictates that the radial stress, σ_r, at the surface of a Si electrode vanishes all the time. Also, the radial stress, σ_r is always equal to the hoop stress σ_θ in the Li-poor phase, due to the symmetry of the system.

3)　Both the radial stress σ_r and hoop stress σ_θ in the Li-poor phase change from tension to compression, as the lithiation proceeds.

Further, to visualize the evolution of the hoop stress in the time domain, Figure 5 plots the hoop stress at the center and at the surface of the Si electrode with respect to the lithiation time. It is seen that the hoop stress at the center is positive, increases to a (positive) maximum at the initial stage, and then changes its sign, i.e., decreases quickly to a negative value. In contrast, the hoop stress at the surface is initially

negative, reaches a (negative) maximum, then starts to reverse and becomes positive rapidly. At the initial stage of lithiation, compressive plastic yielding occurs near the surface layer that undergoes large compressive stress. As the lithiation proceeds, the newly lithiated region at the moving phase boundary starts to expand. However, the surface layer has already been fully lithiated and thus acts as a thin shell to constrain the expansion occurring at the moving phase boundary inside the Si electrode. As a result, a tensile hoop stress is generated near the surface layer, resembling the inflation of a balloon causing the wall stretch.

Phase boundary width.— The phase-field model can yield a phase boundary between the Li-poor and Li-rich phases with a well-defined boundary width λ, while such an essential material length scale is missing in the previous non-linear diffusion model. The phase boundary width can be theoretically estimated according to[30]

$$\lambda = (\hat{c}_\beta - \hat{c}_\alpha)\sqrt{\kappa/2\Delta g} = 1.12 \text{ nm}, \qquad [40]$$

where $\hat{c}_\alpha$ and $\hat{c}_\beta$ are the normalized Li concentration of the Li-poor and Li-rich phases, respectively, as indicated in Figure 2b; κ is the gradient energy coefficient defined earlier; and Δg is the barrier height in the chemical free energy shown in Figure 2b. The theoretical value of λ
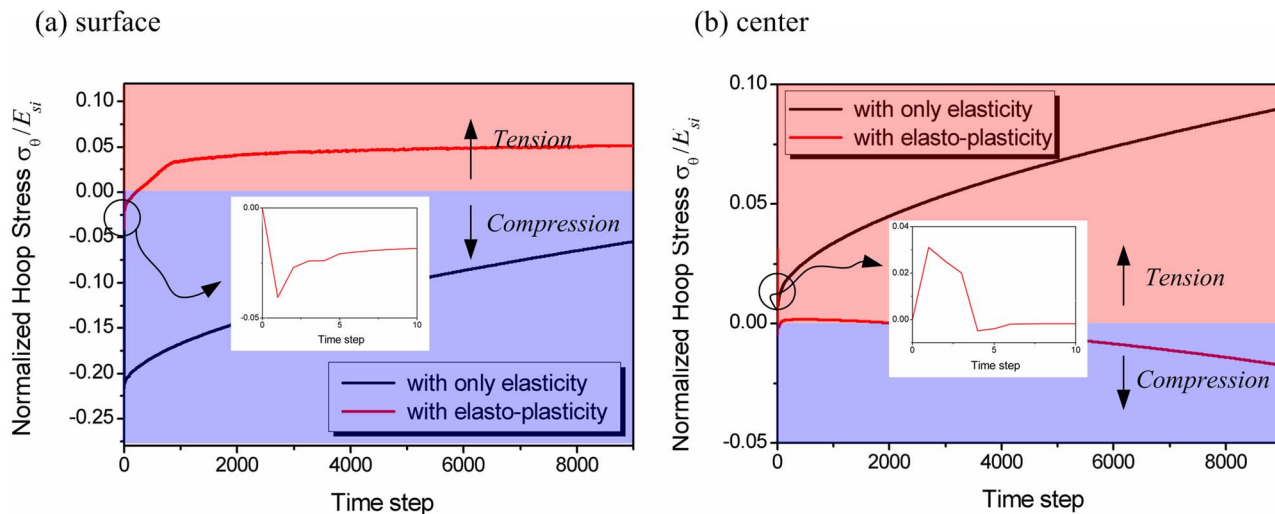
(a) surface

(b) center

Figure 5. The evolution of the hoop stress, σ_θ, at the (a) surface and (b) center of Si electrode. All the stress components are normalized by Young's modulus of Si, E_{si}.
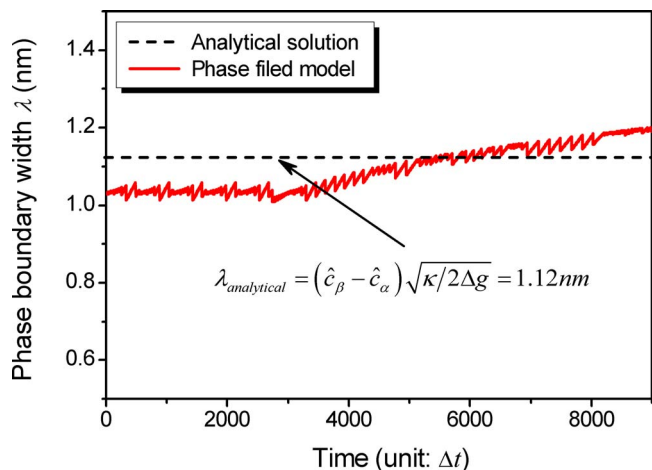

Figure 6. Comparison of evolution of phase boundary width, λ, from the analytical estimate and phase-field model.

agrees well with the experimental measurement, and it also provides a basis for the validation of the present phase-field model.

Figure 6 shows the evolution of phase boundary width λ from the present phase-field model, which is compared with the theoretical estimation. The simulation result is consistent with the theoretical value during the entire lithiation process. More importantly, in the non-linear diffusion model, the phase boundary width can increase to several times the initial value with lithiation. In contrast, the variation of phase boundary width in the present phase-field model is almost negligible. Hence, the material length scale related to this phase boundary thickness is well captured by the present phase-field model.

Effect of plasticity on stress evolution.— In order to illustrate the effect of plasticity, we compare the results of pure elasticity and elasto-platicity. Figure 7 shows the radial distribution of three stress components at $t = 500\Delta t$ and $t = 9000\Delta t$. The solid and dashed lines represent, respectively, the stresses distribution from the pure elasticity and elasto-plasticity models. In addition, Figure 5 shows the hoop stress evolution at both the center and surface of the Si electrode
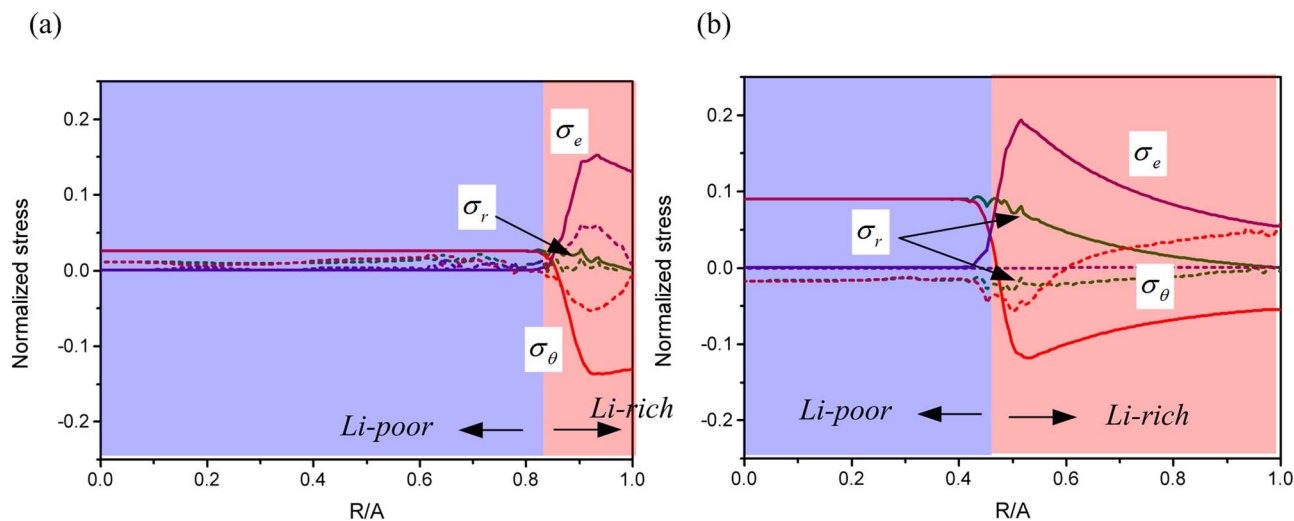
(a)

(b)

Figure 7. The effect of plasticity on radial distributions of the von Mises effective stress, σ_e, radial stress, σ_r and hoop stress σ_θ at different lithiation times of (a) $t = 500\Delta t$, (b) $t = 9000\Delta t$. The solid and dash lines represent, respectively, the stresses distributions by the models with only elasticity and with elasto-plasticity. All the stress components are normalized by Young's modulus of Si, E_{si}.
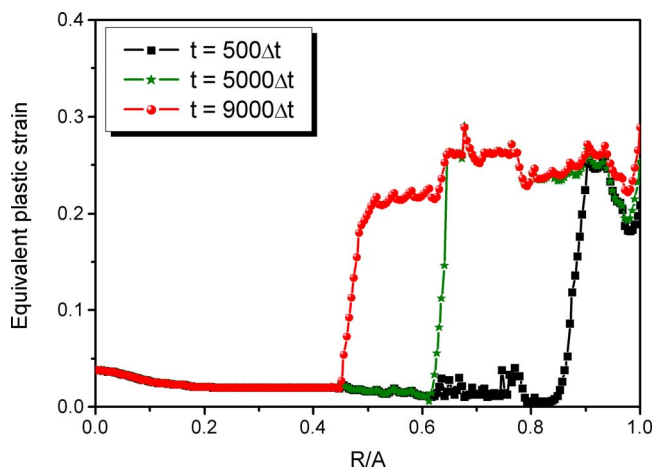
Figure 8. Radial distribution of equivalent plastic strain at different lithiation moments.

during the entire lithiation process. As expected, plastic yielding significantly reduces the stress levels at all lithiation stages. Plasticity also alters the distribution of stress. In comparison, in the absence of plasticity, the hoop stress σ_θ is always compressive at the surface layer of the Si electrode and tensile in the Li-poor phase. This result implies that fracture would initiate at the center of the Li-poor phase, which contradicts with both the experimental observations and the prediction with plasticity included (as discussed in detail previously), that is, the reversal of hoop compression to tension in the surface layer.

Another interesting observation is that the central region of the Si electrode, corresponding to the Li-poor phase, remains elastic. More specifically, from the radial distribution of equivalent plastic strain at different lithiation moments, shown in Figure 8, it is clear that the boundary between the elastic and plastic regions moves toward the center in the Si electrode, in consistent with the movement of the phase boundary (i.e., the abrupt change of the Li concentration profile) in Figure 3. Interestingly, the center region still remains elastic even at the late stage. This is because the stress field near the center region is almost hydrostatic ($\sigma_e = |\sigma_r - \sigma_\theta| = 0$), which does not facilitate plastic deformation in terms of the deviatoric stress-dependent yielding criterion.

Conclusions

We have developed a phase-field model coupled with large elasto-plastic deformation in an open system. The model accounts for the concurrent processes of material insertion, phase change, and large elasto-plastic swelling. The concentration profiles and deformation geometries were co-evolved by a set of integrated phase-field and mechanics equations. In order to facilitate the study of complex geometries and boundary conditions, these equations are numerically solved by the finite element method.

As an example, the phase-field model was applied to studying the stress evolution in a *c*-Si electrode upon lithiation. It is shown that as the lithiation proceeds, the hoop stress can change from the initial compression to tension in the surface layer of a Si electrode, which explains the experimentally observed surface cracking.

The sharp phase boundary between the Li-poor and Li-rich phases is naturally captured in the present phase-field model, in contrast to the previous non-linear diffusion model where an elaborate interfacial domain is needed to model the phase boundary. The phase boundary width in the present model is shown to be nearly unchanged during lithiation, in contrast to the non-linear diffusion model where the phase boundary width changes with the lithiation extent.

Finally, we note that the present phase-field model is thermodynamically consistent, thus enabling a full chemo-mechanical coupling.

Our model allows the phase-field method to simultaneously account for the stress induced by lithiation as well as the Li transport mediated by stress. A systematic investigation of the coupling between stress and Li diffusion/reaction kinetics is beyond the scope of this study, and will be reported in a forthcoming publication. Our phase-field model is generally applicable to the high-capacity electrode systems undergoing large elasto-plastic deformation.[23,45,46]

References

1. V. A. Sethuraman, L. J. Hardwick, V. Srinivasan, and R. Kostecki, *Journal of Power Sources*, **195**, 3655 (2010).
2. J.-M. Tarascon and M. Armand, *Nature*, **414**, 359 (2001).
3. C. K. Chan, H. Peng, G. Liu, K. McIlwrath, X. F. Zhang, R. A. Huggins, and Y. Cui, *Nature nanotechnology*, **3**, 31 (2008).
4. X. H. Liu, F. Fan, H. Yang, S. Zhang, J. Y. Huang, and T. Zhu, *Acs Nano*, **7**, 1495 (2013).
5. X. H. Liu, J. W. Wang, S. Huang, F. Fan, X. Huang, Y. Liu, S. Krylyuk, J. Yoo, S. A. Dayeh, and A. V. Davydov, *Nature nanotechnology*, **7**, 749 (2012).
6. M. T. McDowell, I. Ryu, S. W. Lee, C. Wang, W. D. Nix, and Y. Cui, *Advanced Materials*, **24**, 6034 (2012).
7. J. W. Wang, Y. He, F. Fan, X. H. Liu, S. Xia, Y. Liu, C. T. Harris, H. Li, J. Y. Huang, and S. X. Mao, *Nano Letters*, **13**, 709 (2013).
8. L.-F. Cui, R. Ruffo, C. K. Chan, H. Peng, and Y. Cui, *Nano Letters*, **9**, 491 (2008).
9. X. H. Liu, H. Zheng, L. Zhong, S. Huang, K. Karki, L. Q. Zhang, Y. Liu, A. Kushima, W. T. Liang, J. W. Wang, J.-H. Cho, E. Epstein, S. A. Dayeh, S. T. Picraux, T. Zhu, J. Li, J. P. Sullivan, J. Cumings, C. Wang, S. X. Mao, Z. Z. Ye, S. Zhang, and J. Y. Huang, *Nano Letters*, **11**, 3312 (2011).
10. X. H. Liu, L. Zhong, S. Huang, S. X. Mao, T. Zhu, and J. Y. Huang, *Acs Nano*, **6**, 1522 (2012).
11. M. J. Chon, V. A. Sethuraman, A. McCormick, V. Srinivasan, and P. R. Guduru, *Physical Review Letters*, **107**, 045503 (2011).
12. A. F. Bower, P. R. Guduru, and V. A. Sethuraman, *Journal of the Mechanics and Physics of Solids*, **59**, 804 (2011).
13. H. Haftbaradaran, J. Song, W. Curtin, and H. Gao, *Journal of Power Sources*, **196**, 361 (2011).
14. Y. Yao, M. T. McDowell, I. Ryu, H. Wu, N. Liu, L. Hu, W. D. Nix, and Y. Cui, *Nano Letters*, **11**, 2949 (2011).
15. K. Zhao, M. Pharr, J. J. Vlassak, and Z. Suo, *Journal of Applied Physics*, **109**, 016110 (2011).
16. J. L. Goldman, B. R. Long, A. A. Gewirth, and R. G. Nuzzo, *Advanced Functional Materials*, **21**, 2412 (2011).
17. V. A. Sethuraman, V. Srinivasan, A. F. Bower, and P. R. Guduru, *Journal of the Electrochemical Society*, **157**, A1253 (2010).
18. A. Bower and P. Guduru, *Modelling and Simulation in Materials Science and Engineering*, **20**, 045004 (2012).
19. Z. Cui, F. Gao, and J. Qu, *Journal of the Mechanics and Physics of Solids*, **60**, 1280 (2012).
20. V. Shenoy, P. Johari, and Y. Qi, *Journal of Power Sources*, **195**, 6825 (2010).
21. K. Zhao, M. Pharr, S. Cai, J. J. Vlassak, and Z. Suo, *Journal of the American Ceramic Society*, **94**, s226 (2011).
22. Y. An and H. Jiang, *Modelling and Simulation in Materials Science and Engineering*, **21**, 074007 (2013).
23. M. Gu, H. Yang, D. E. Perea, J.-G. Zhang, S. Zhang, and C. Wang, *Nano Letters* (2014).
24. Z. Cui, F. Gao, and J. Qu, *Journal of the Mechanics and Physics of Solids*, **61**, 293 (2013).
25. S. Huang, F. Fan, J. Li, S. Zhang, and T. Zhu, *Acta materialia*, **61**, 4354 (2013).
26. S. Huang and T. Zhu, *Journal of Power Sources*, **196**, 3664 (2011).
27. H. Yang, S. Huang, X. Huang, F. Fan, W. Liang, X. H. Liu, L.-Q. Chen, J. Y. Huang, J. Li, and T. Zhu, *Nano Letters*, **12**, 1953 (2012).
28. H. Yang, X. Huang, T. Zhu, and S. Zhang, *Journal of the Mechanics and Physics of Solids* (2014).
29. I. Steinbach and M. Apel, *Physica D: Nonlinear Phenomena*, **217**, 153 (2006).
30. L.-Q. Chen, *Annual review of materials research*, **32**, 113 (2002).
31. Y. Suwa, Y. Saito, and H. Onodera, *Computational materials science*, **44**, 286 (2008).
32. S. Hu and L. Chen, *Acta materialia*, **49**, 1879 (2001).
33. C. Krill Iii and L.-Q. Chen, *Acta materialia*, **50**, 3059 (2002).
34. A. Van der Ven, K. Garikipati, S. Kim, and M. Wagemaker, *Journal of the Electrochemical Society*, **156**, A949 (2009).
35. M. Z. Bazant, *Accounts of chemical research*, **46**, 1144 (2013).
36. D. A. Cogswell and M. Z. Bazant, *Acs Nano*, **6**, 2215 (2012).
37. L. Anand, *Journal of the Mechanics and Physics of Solids*, **60**, 1983 (2012).

38. C. V. Di Leo, E. Rejovitzky, and L. Anand, *Journal of the Mechanics and Physics of Solids* (2014).
39. T. Belytschko, W. K. Liu, B. Moran, and K. Elkhodary, *Nonlinear finite elements for continua and structures*, John Wiley & Sons (2013).
40. J. Eshelby, *Journal of Elasticity*, **5**, 321 (1975).
41. J. D. Eshelby, *Philosophical Transactions of the Royal Society of London. Series A, Mathematical and Physical Sciences*, **244**, 87 (1951).
42. F. Larché and J. Cahn, *Acta Metallurgica*, **21**, 1051 (1973).
43. Q. Zhang, W. Zhang, W. Wan, Y. Cui, and E. Wang, *Nano Letters*, **10**, 3243 (2010).
44. V. A. Sethuraman, M. J. Chon, M. Shimshak, V. Srinivasan, and P. R. Guduru, *Journal of Power Sources*, **195**, 5062 (2010).
45. W. Liang, L. Hong, H. Yang, F. Fan, Y. Liu, H. Li, J. Li, J. Y. Huang, L.-Q. Chen, and T. Zhu, *Nano Letters*, **13**, 5212 (2013).
46. W. Liang, H. Yang, F. Fan, Y. Liu, X. H. Liu, J. Y. Huang, T. Zhu, and S. Zhang, *Acs Nano*, **7**, 3427 (2013).